Supporting Information

# $Ba^{2+}$ Co-doping Enhances Phase Purity and Enables Narrow-Band Green Emission in $Sr_{5/6}Li_{17/6}Al_{7/6}O_4:Eu^{2+}$ Phosphor for Backlight Display Applications

Chenyang Zhan[a,b], Zihao Wang[a,b], Sisi Liang[a,b], Zhiying Zhao[a,b], Hanru Chen[a,b], Jiahe Yu[a,b,c] and Haomiao Zhu[a,b*]

[a] State Key Laboratory of Structural Chemistry, Fujian Institute of Research on the Structure of Matter, Chinese Academy of Sciences, Fuzhou, Fujian 350108, China

[b] Xiamen Key Laboratory of Rare Earth Photoelectric Functional Materials, Xiamen Institute of Rare Earth Materials, Xiamen 361021, China

[c] College of Chemistry and Materials Science, Fujian Normal University, Fuzhou, Fujian, 350007, China

[*]Corresponding author (email: zhm@fjirsm.ac.cn)

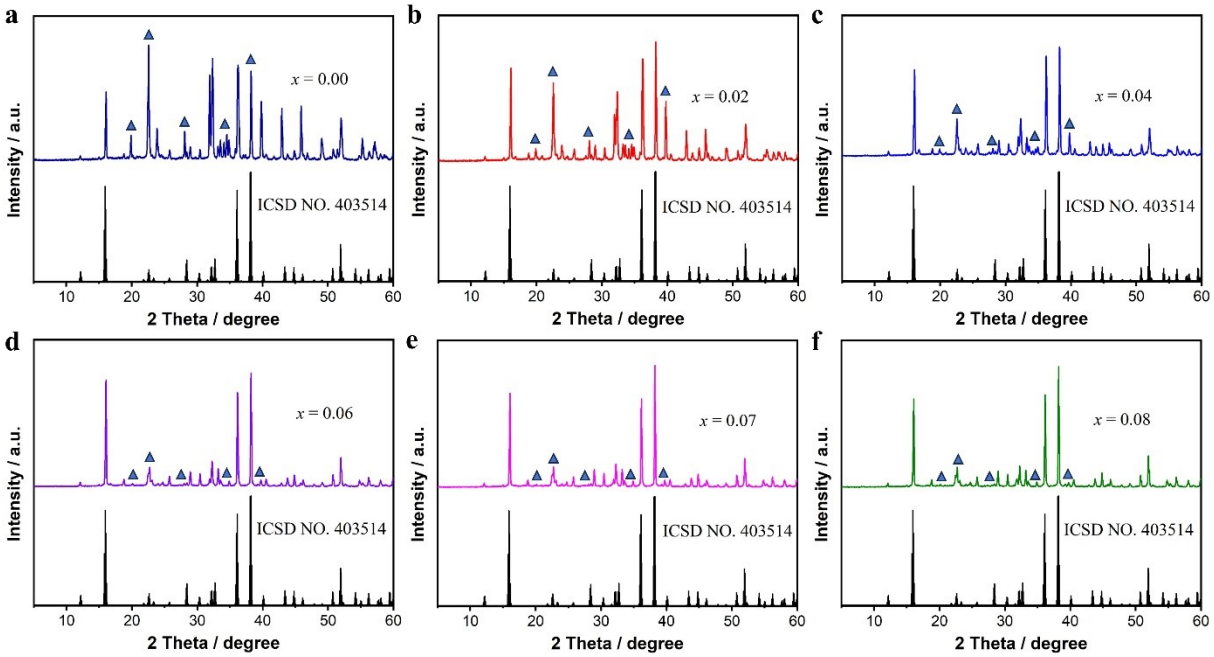


**Fig. S1.** XRD patterns of $Sr_{5/6-x}Ba_xLi_{17/6-x}Al_{7/6}O_4:Eu^{2+}$ (denoted as SBLAO:$Eu^{2+}$) phosphors with varying $Ba^{2+}$ doping concentrations ($x$). As the $Ba^{2+}$ content increases, the characteristic diffraction peaks of impurity phases located at 2θ = 19.89°, 22.59°, 28.09°, 34.56°, and 39.78° progressively weaken and eventually become negligible.

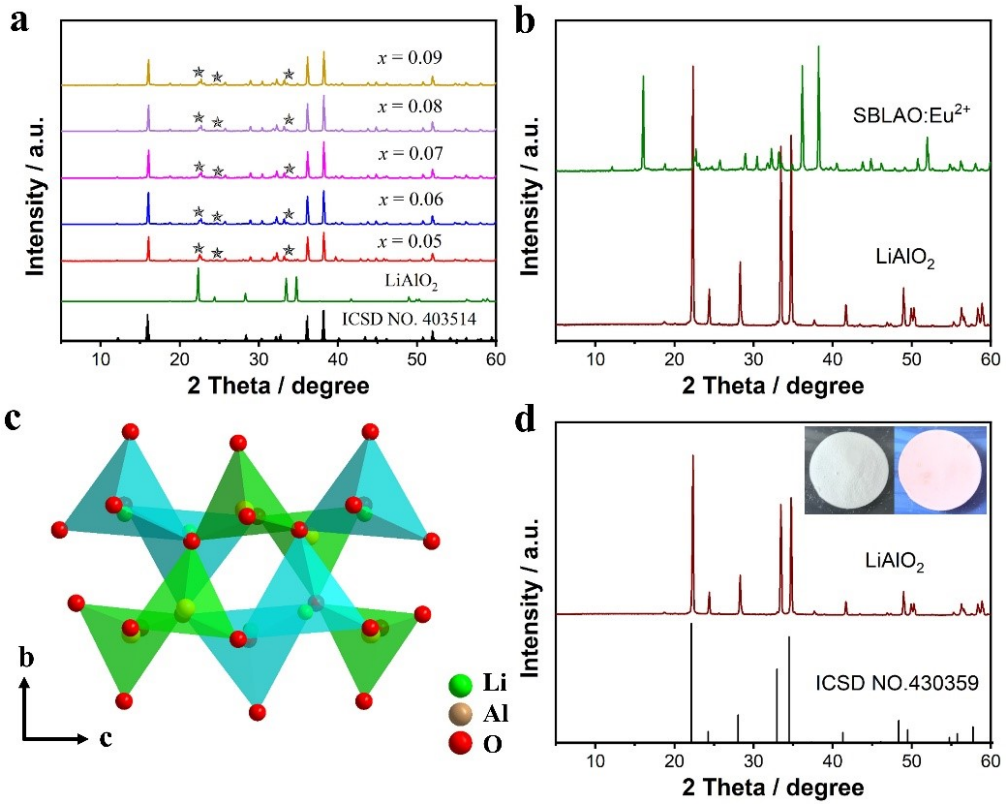


**Fig. S2.** (a) XRD patterns of SBLAO:$Eu^{2+}$ phosphors with varying $Ba^{2+}$ doping concentrations. (b) Comparison of the XRD pattern of the SBLAO:$Eu^{2+}$ sample with $LiAlO_2$ sample. (c) Crystal structure of $LiAlO_2$ viewed along the *a*-axis. (d) XRD pattern of $LiAlO_2$:$Eu^{2+}$ synthesized under the same conditions as SBLAO:$Eu^{2+}$. The insets show photographs of the sample under daylight and 365 nm UV illumination, respectively. Only characteristic weak red emission from $Eu^{3+}$ is observed, confirming that the $LiAlO_2$ impurity phase does not contribute to the $Eu^{2+}$ luminescence.

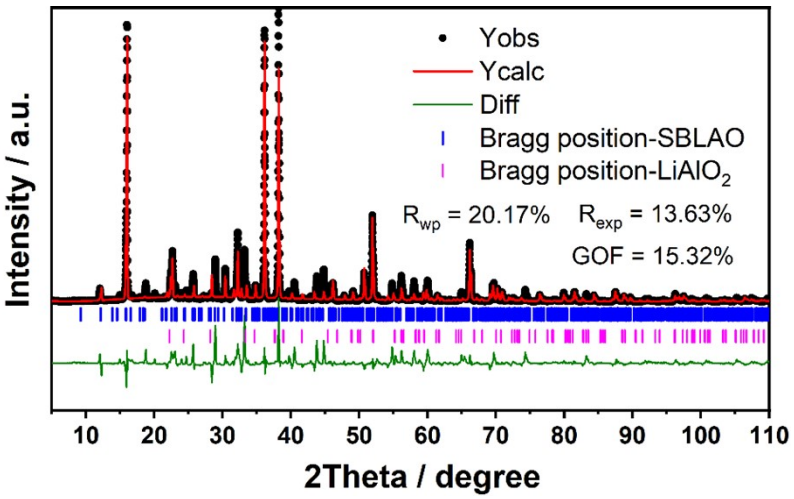


**Fig. S3.** The refinement structure of SBLAO along with their measured data and calculated profiles.

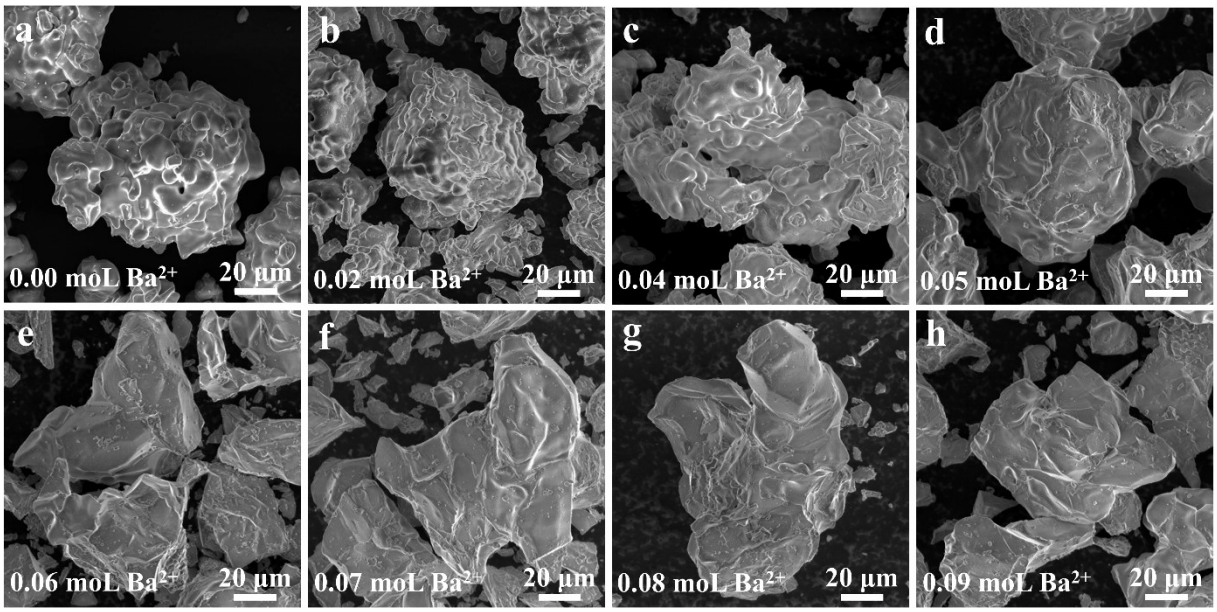


**Fig. S4.** SEM images of SBLAO:$Eu^{2+}$ phosphors synthesized with different $Ba^{2+}$ doping concentrations.

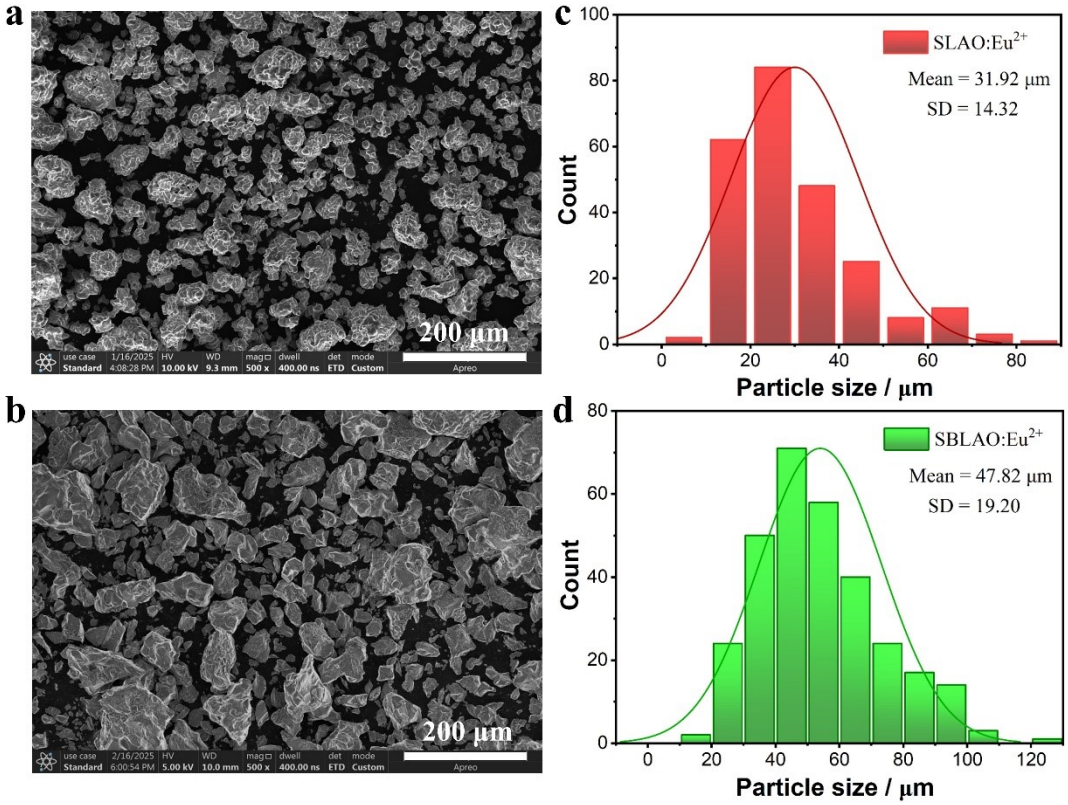


**Fig. S5.** (a,b) SEM images of SLAO:$Eu^{2+}$ and SBLAO:$Eu^{2+}$ phosphors. (c,d) The particle size distribution of SLAO:$Eu^{2+}$ and SBLAO:$Eu^{2+}$ phosphors.

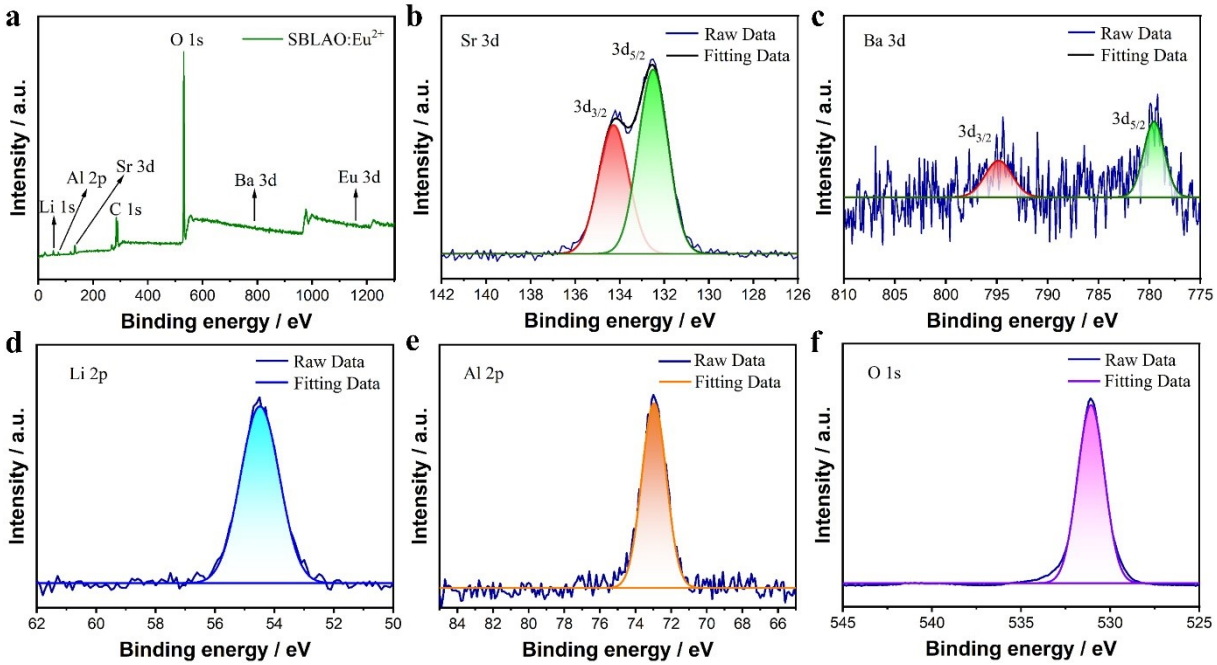


**Fig. S6.** XPS analysis of SBLAO:$Eu^{2+}$. (a) Survey spectrum. (b–f) High-resolution spectra of (b) Sr 3d, (c) Ba 3d, (d) Li 1s, (e) Al 2p, and (f) O 1s core levels. The Sr 3d spectrum exhibits doublet peaks at 132.52 eV ($3d_{5/2}$) and 134.28 eV ($3d_{3/2}$), consistent with $Sr^{2+}$. The Ba 3d spectrum shows peaks at 779.52 eV ($3d_{5/2}$) and 794.86 eV ($3d_{3/2}$), confirming $Ba^{2+}$. The Li 1s peak is observed at 54.52 eV, while the Al 2p peak appears at 72.95 eV, corresponding to $Al^{3+}$. The O 1s spectrum shows a peak centered at 531.09 eV.

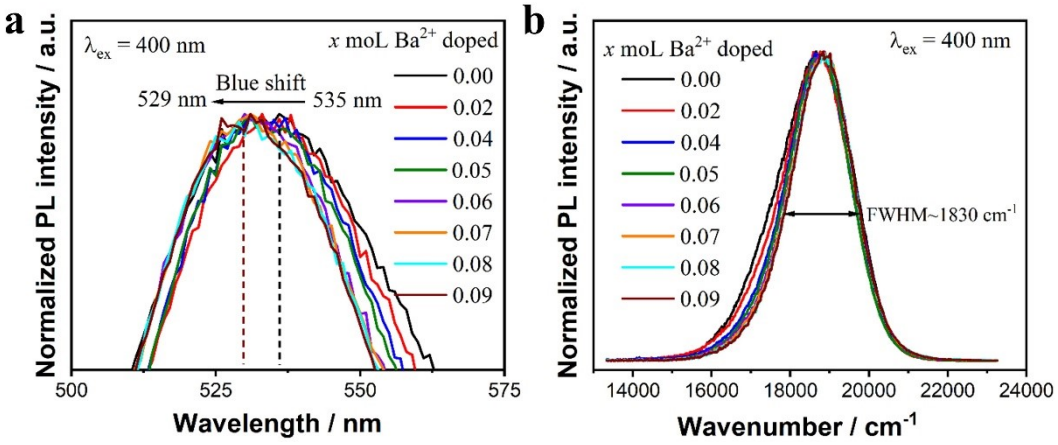


**Fig. S7.** a) Magnified view of the PL spectra of SBLAO:$Eu^{2+}$ phosphors in the wavelength range of 500–575 nm, showing a slight blue shift of the emission peak with increasing $Ba^{2+}$ content. b) Corresponding PL spectra plotted on an energy scale ($cm^{-1}$). The low-energy side of the emission undergoes more significant changes than the high-energy side.

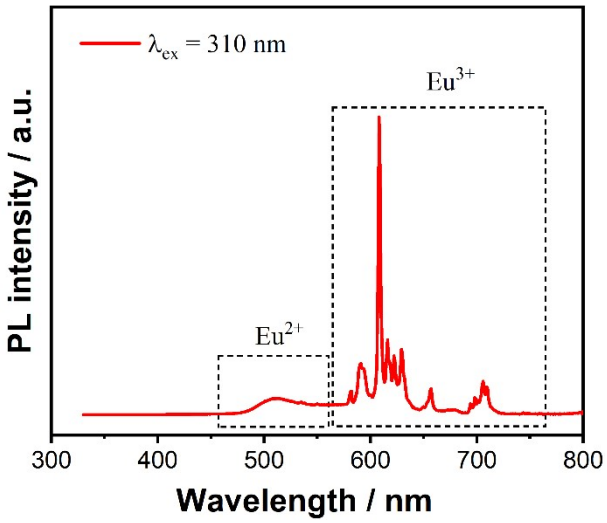


**Fig. S8.** PL spectra of SBLAO:$Eu^{2+}$ phosphor under 310 nm excitation. The rectangles indicate the characteristic emission peaks corresponding to $Eu^{2+}$ and $Eu^{3+}$.

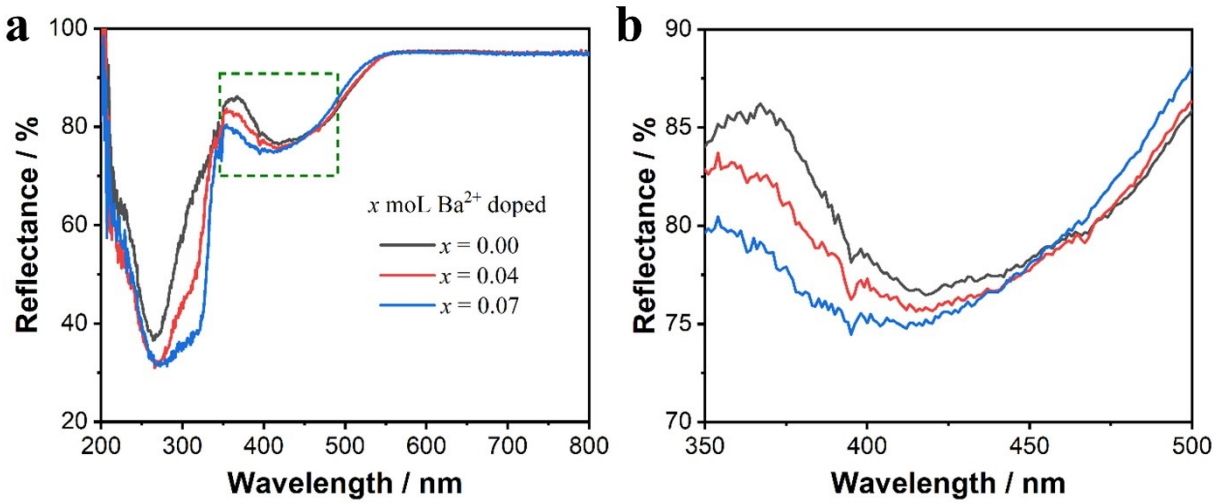


**Fig. S9.** (a) Diffuse reflectance spectra of SBLAO:$Eu^{2+}$ phosphors with varying $Ba^{2+}$ doping concentrations. (b) Magnified view of the region within the 350–500 nm range indicated in (a).

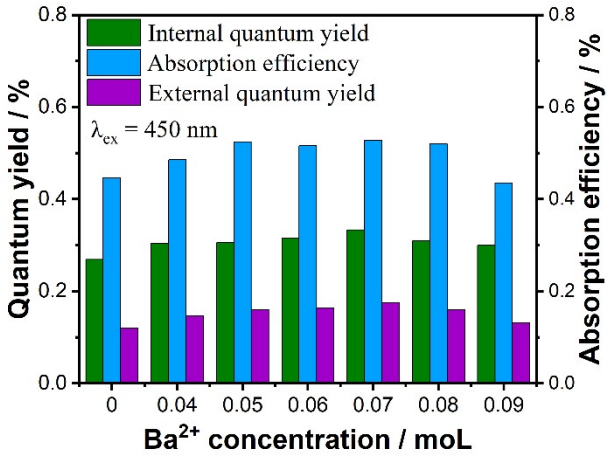


**Fig. S10.** PL quantum yield and absorption efficiency as a function of $Ba^{2+}$ concentration under 450 nm excitation.

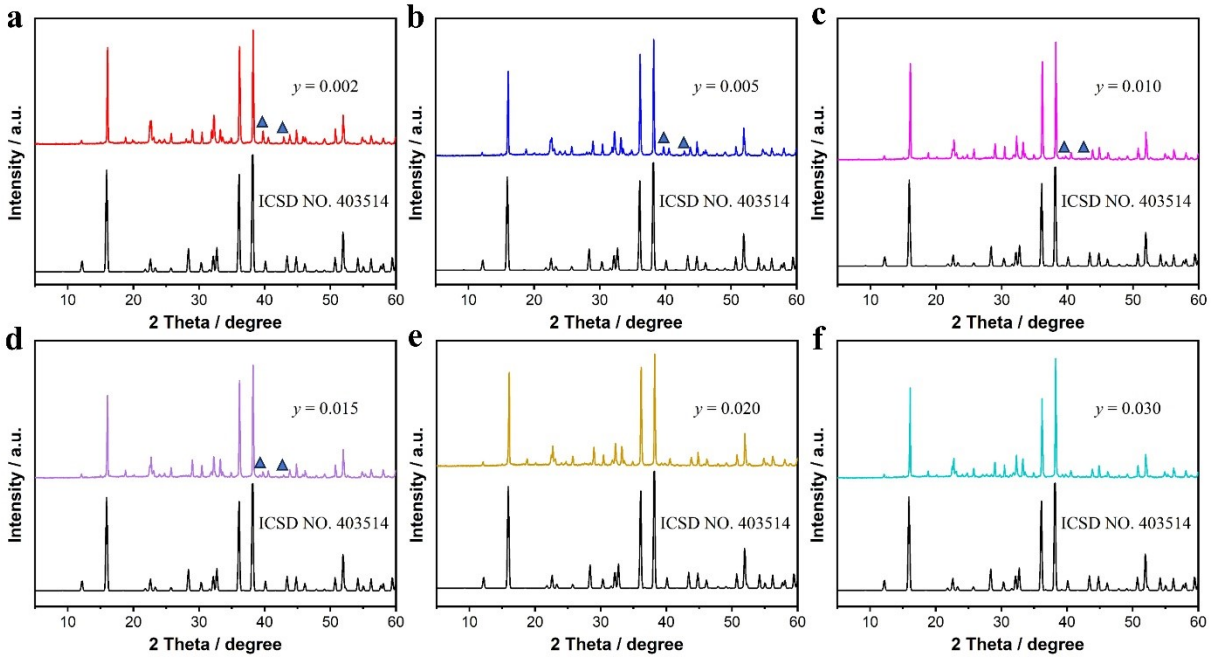


**Fig. S11.** XRD patterns of SBLAO:$Eu^{2+}$ phosphors synthesized with different $Eu^{2+}$ doping concentrations ($y$). As the $Eu^{2+}$ content increases, the characteristic diffraction peaks of impurity phases located at $2\theta = 39.78°$ and $42.88°$ progressively weaken and eventually become negligible.

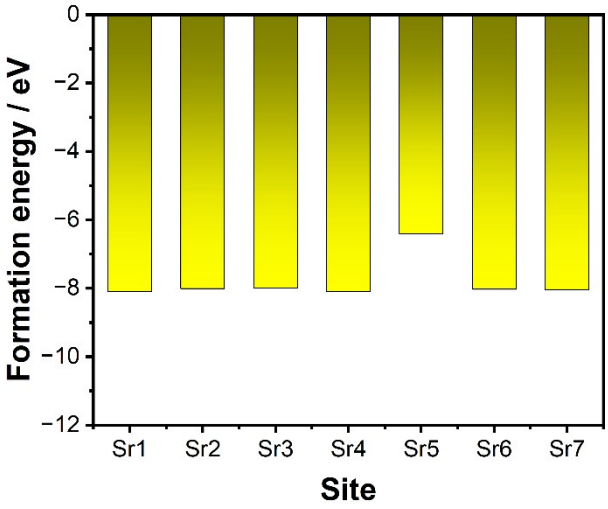


**Fig. S12.** Formation energies for $Eu^{2+}$ substitution at various Sr sites in SLAO, calculated via first-principles computations within the Vienna Ab initio Simulation Package (VASP). The substitution formation energy per defect, $E_f$ is defined as:

$$E_f = \frac{E_d - (E_P - n\mu_Y + n\mu_X)}{n}$$

where $E_d$ and $Ep$ denote the total energies of the doped and pristine systems, respectively, $n$ is the number of substituted atoms, and $\mu_X$ and $\mu_Y$ represent the chemical potentials of the impurity (Eu) and the host atom (Sr), respectively.

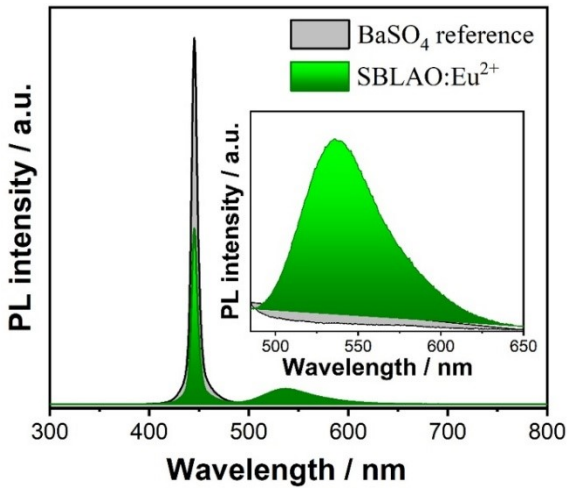


**Fig. S13.** Excitation profile of $BaSO_4$ and PL spectra of SBLAO:$Eu^{2+}$ measured with an integrating sphere under 450 nm excitation; the inset shows a magnified view.

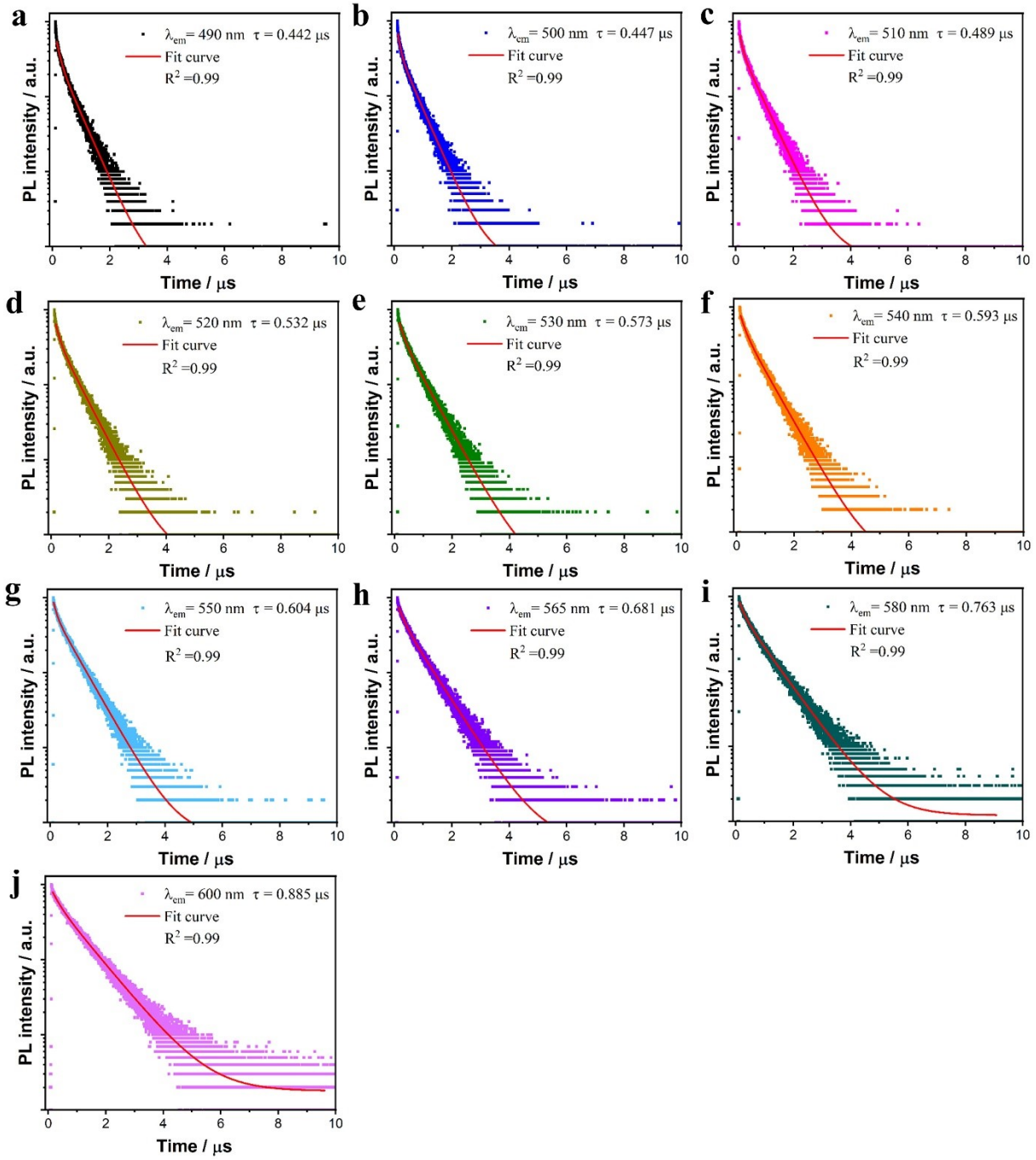


**Fig. S14.** PL decay curve and fitting results of SBLAO:$Eu^{2+}$ phosphor monitored at different wavelength.

The decay curves were fitted using bi-exponential function:

$$I(t) = \sum_{i=1}^{n} A_i exp\left(-\frac{t}{\tau_i}\right), n = 1, 2$$

where $I(t)$ represents the luminescence intensity at time $t$, $\tau_i$ denotes the lifetime of various components, and $A_i$ is a constant.

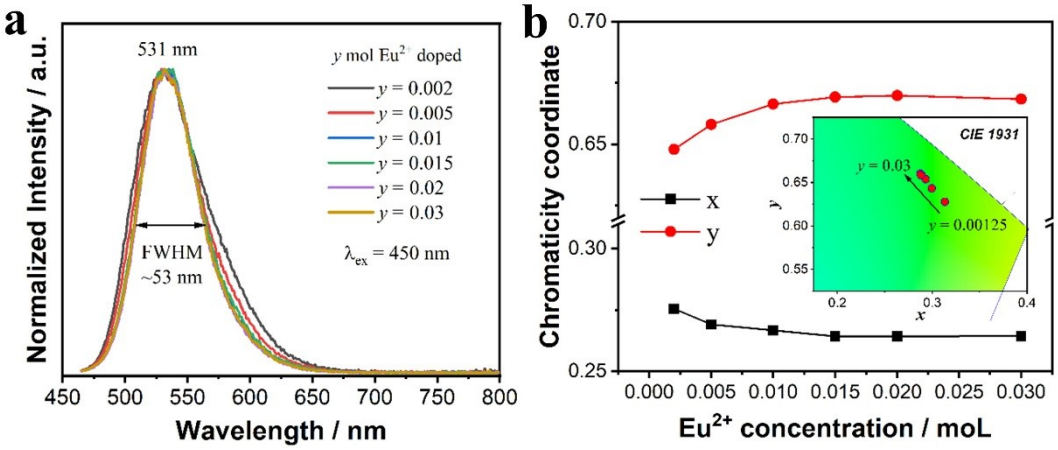


**Fig. S15.** (a) Normalized PL spectra as a function of $Eu^{2+}$ concentration under 450 nm excitation. (b) Shift of chromaticity coordinates ($x$, $y$) in the CIE 1931 color space.

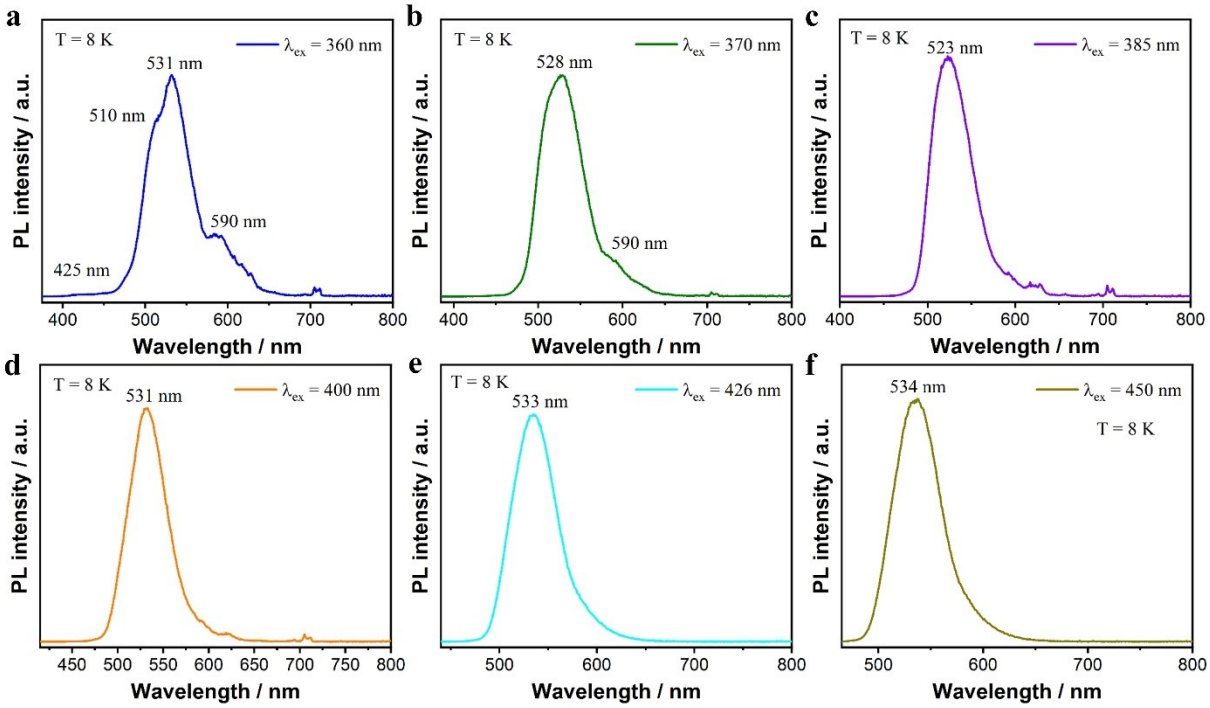


**Fig. S16.** Low-temperature (8 K) PL spectra of SBLAO:$Eu^{2+}$ measured under selected excitation wavelengths: (a) 360 nm, (b) 370 nm, (c) 385 nm, (d) 400 nm, (e) 426 nm, and (f) 450 nm.

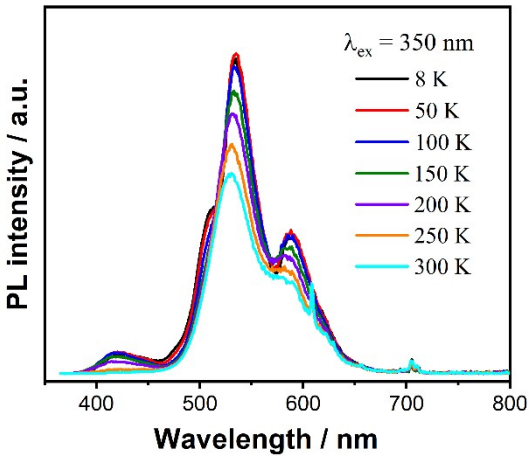


**Fig. S17.** Temperature-dependent PL spectra of SBLAO:$Eu^{2+}$ measured from 8 to 300 K under 350 nm excitation.

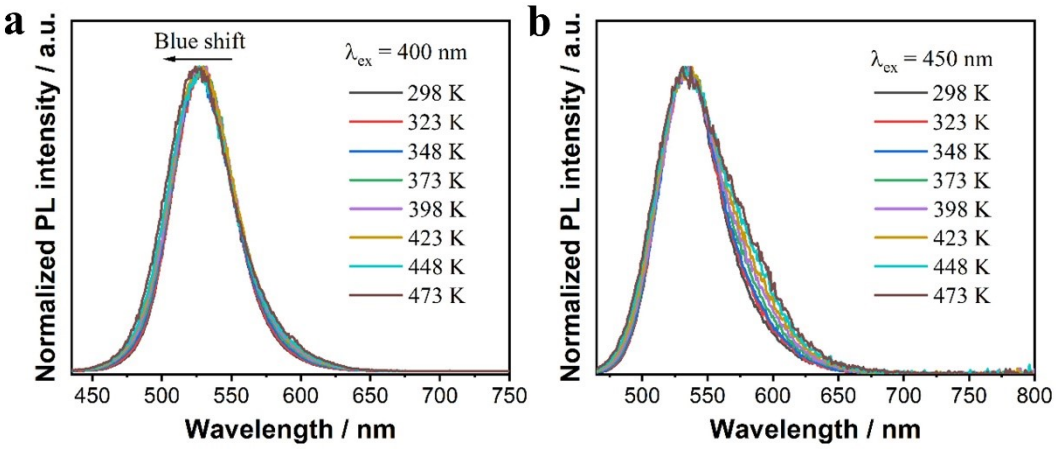


**Fig. S18.** .Normalized PL spectra as a function of temperature (298–473 K) under excitation at (a) 400 nm and (b) 450 nm.

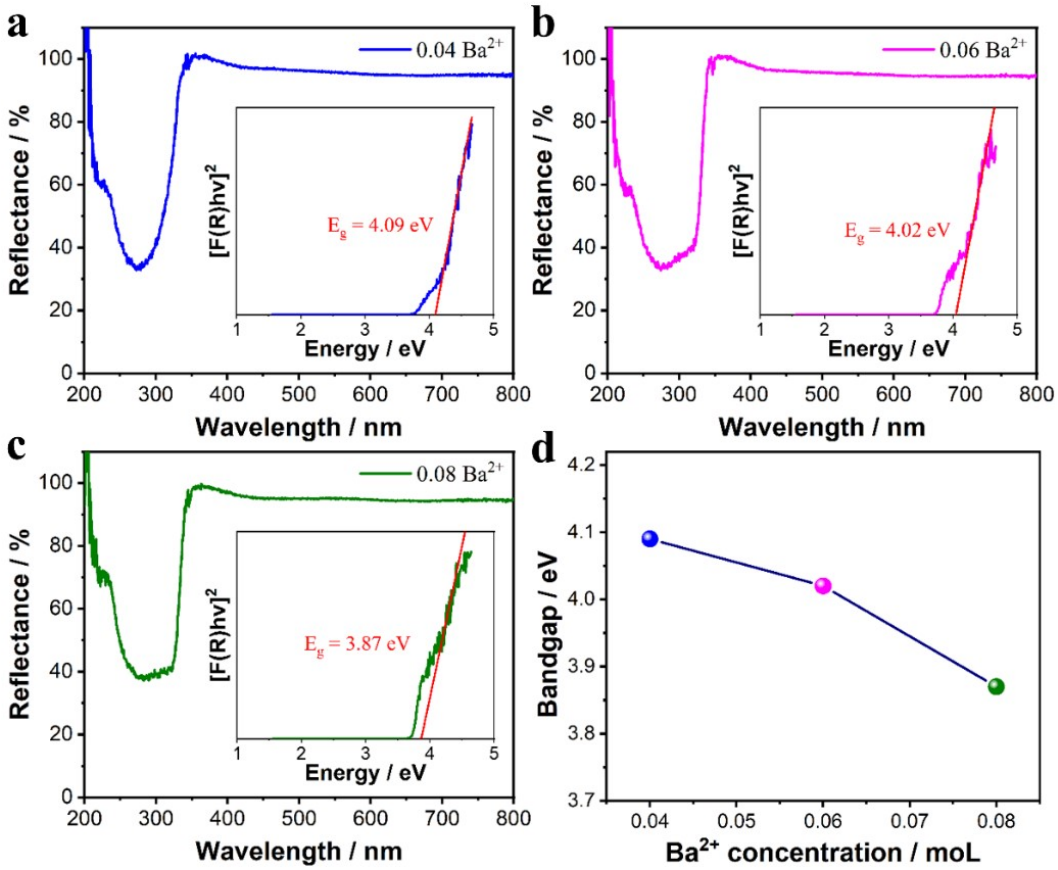


**Figure S19.** (a-c) Diffuse reflectance spectra of SBLAO hosts with varying $Ba^{2+}$ doping concentrations ($x$ = 0.04, 0.06, and 0.08 moL). The insets show the corresponding Tauc plots for direct bandgap estimation. (d) The extracted bandgap energy ($E_g$) as a function of $Ba^{2+}$ concentration, determined from the corresponding Tauc plots (insets in a–c). Note that samples with low $Ba^{2+}$ doping ($x$ < 0.04 moL) were excluded from this analysis due to the presence of minor impurity phases, which could affect the accuracy of bandgap determination.

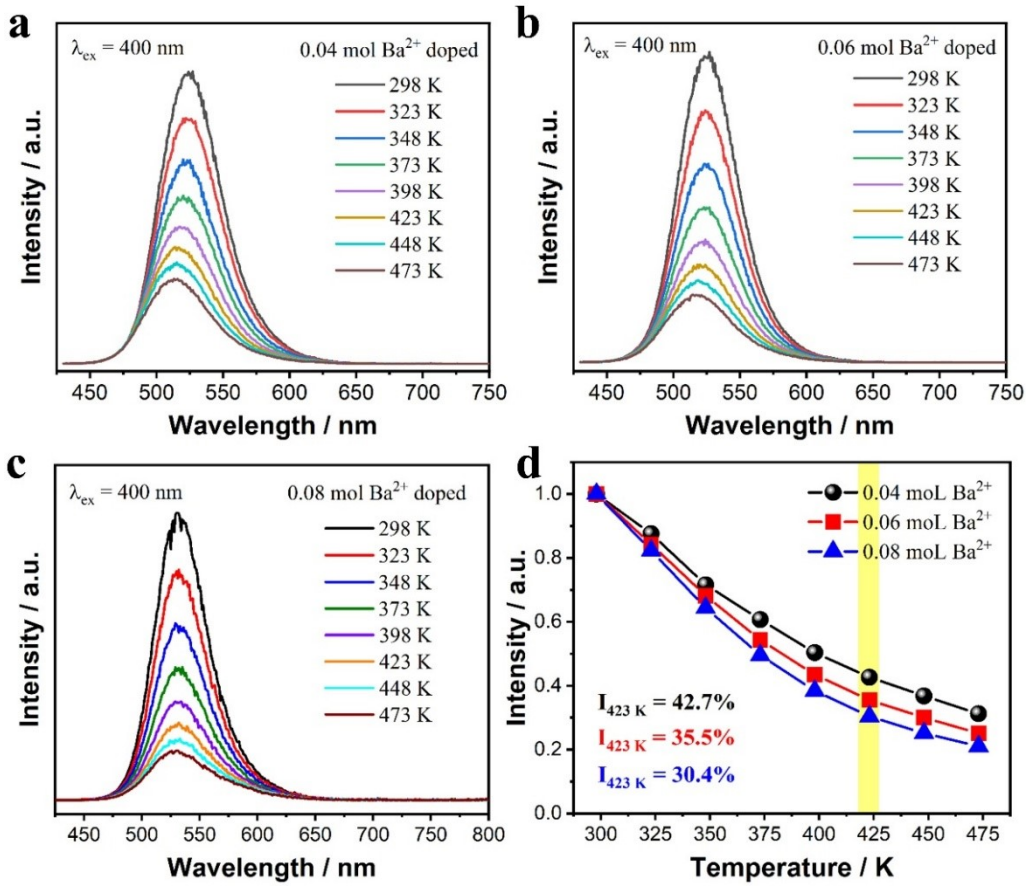


**Figure S20.** Temperature-dependent luminescence properties of SBLAO:$Eu^{2+}$ phosphors with different $Ba^{2+}$ doping concentrations. (a–c) PL spectra measured from 298 to 473 K under 400 nm excitation for $x$ = 0.04, 0.06, and 0.08 moL, respectively. (d) Comparison of the normalized integrated PL intensity as a function of temperature for the three samples.

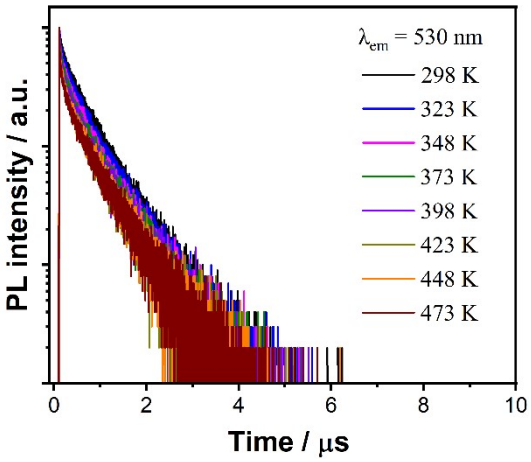


**Fig. S21.** Temperature-dependent PL decay curves of SBLAO:$Eu^{2+}$ phosphor monitored at 530 nm from 298 to 473 K.

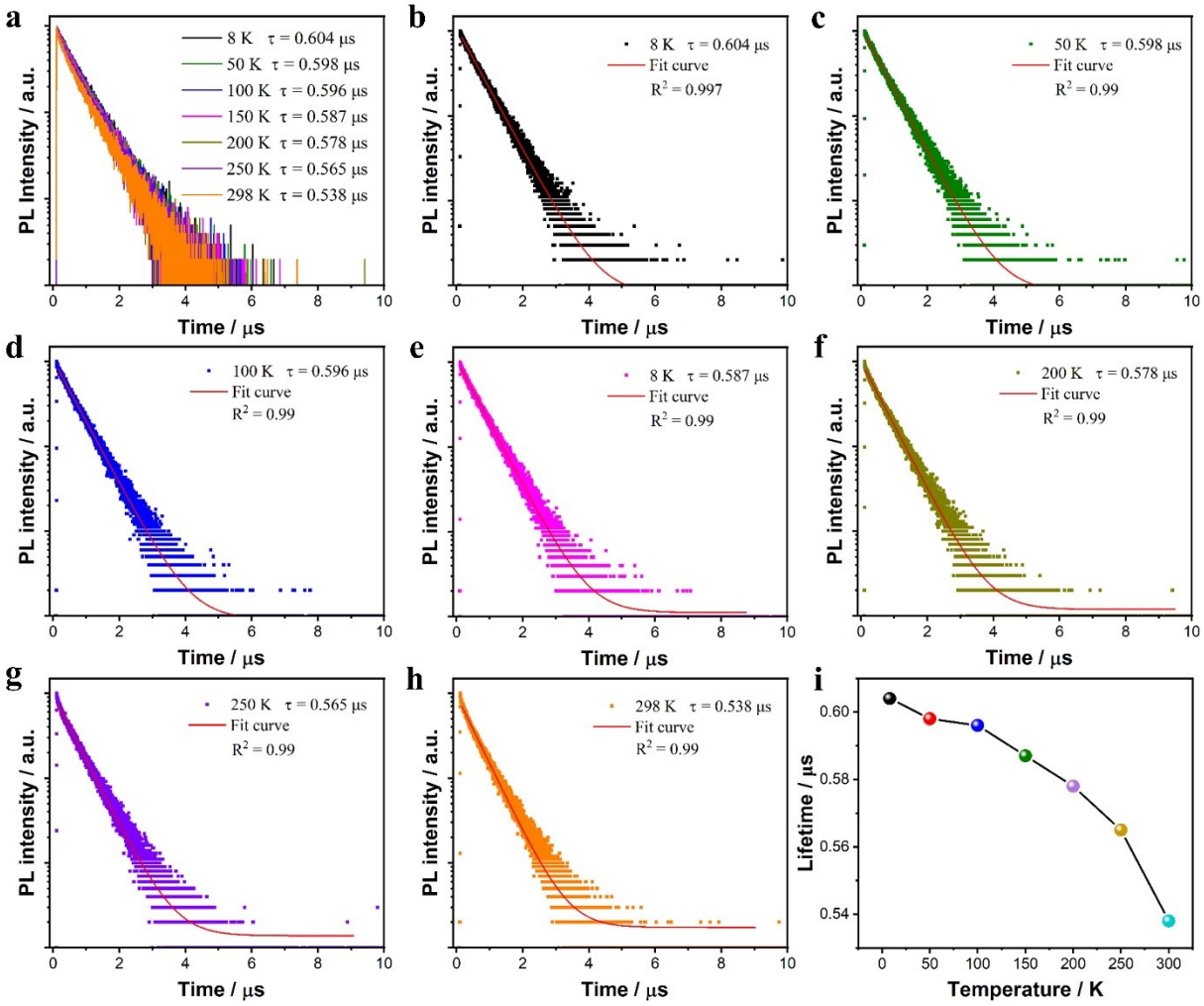


**Fig. S22.** (a) Temperature-dependent PL decay curves of SBLAO:$Eu^{2+}$ phosphor monitored at 530 nm from 8 to 298 K. (b–h) PL decay curves and corresponding fitting results at selected temperatures: (b) 8 K, (c) 50 K, (d) 100 K, (e) 150 K, (f) 200 K, (g) 250 K, and (h) 298 K. (i) Temperature dependence of the emission lifetime extracted from the fitted decay curves.

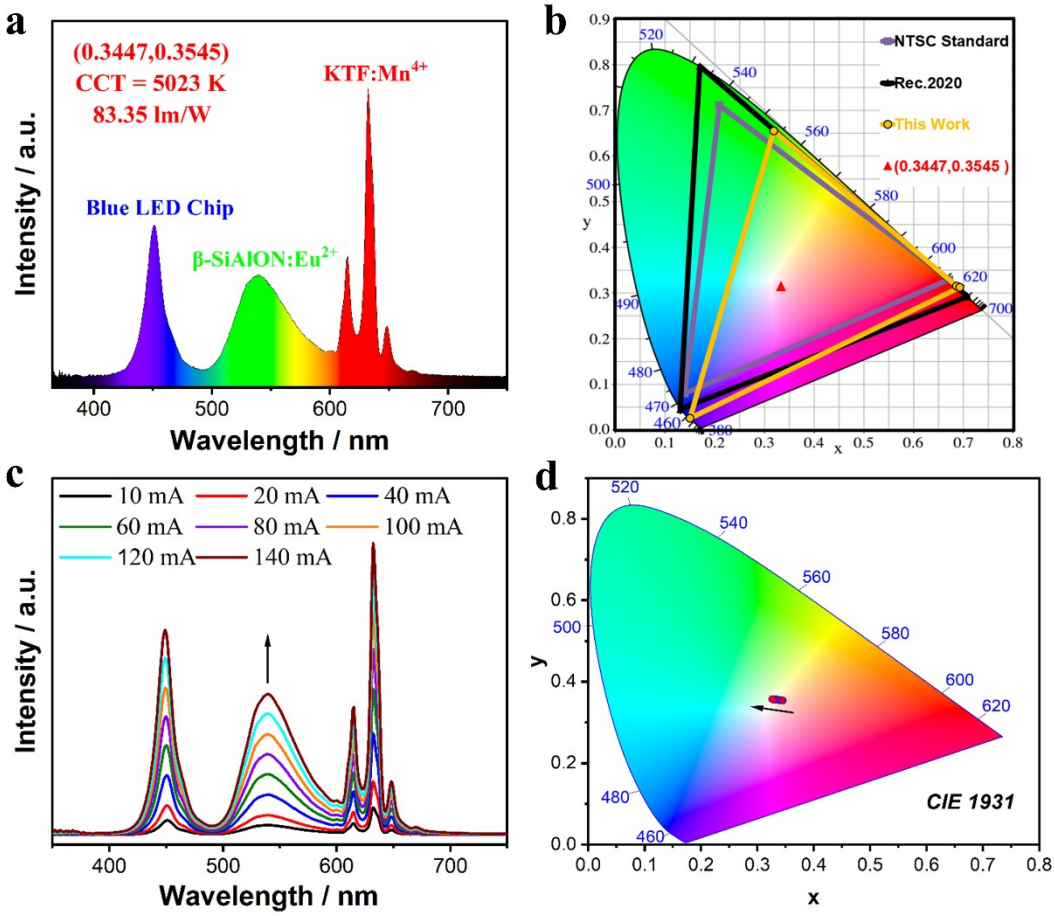


**Fig. S23.** (a) Electroluminescence (EL) spectrum of the wLED device fabricated with the green phosphor β-SiAlON:$Eu^{2+}$, red phosphor $K_2TiF_6$:$Mn^{4+}$, and a blue InGaN chip ($\lambda_{em}$ = 450 nm) under a current of 10 mA. (b) CIE 1931 color coordinate of the fabricated wLED, color space of NTSC standard, Rec. 2020 standard, and wLED device. (c) EL spectra of the LED device under various driving currents. (d) The change of CIE chromaticity coordinates under various driving currents.

**Table S1.** The polyhedral coordination parameters of Sr ions in the channel.

| Polyhedra | Symmetry | S.O.F | $d_{min}$[a)] (Å) | $d_{max}$[a)] (Å) | $V$[b)] (Å$^3$) |
|---|---|---|---|---|---|
| Sr1 | $C_4$ | 1 | 2.570 | 2.774 | 29.245 |
| Sr2 | $C_4$ | 0.653(7) | 2.544 | 3.007 | 31.609 |
| Sr3 | $C_4$ | 0.299(9) | 2.487 | 3.182 | 32.965 |
| Sr4 | $C_4$ | 0.176(12) | 2.606 | 2.964 | 32.965 |
| Sr5 | $C_4$ | 0.872(4) | 2.547 | 2.895 | 30.276 |
| Sr6 | $C_4$ | 1 | 2.631 | 2.683 | 28.707 |
| Sr7 | $C_4$ | 1 | 2.645 | 2.659 | 28.379 |

a) $d_i$ is the distance from the center atom to the $i$th coordination atom.

b) $V$ is the volume of polyhedron.

**Table S2.** Chromaticity coordinates ($x$, $y$) of SBLAO:$Eu^{2+}$ with varying $Ba^{2+}$ doping concentrations ($x$) in the CIE 1931 color space under 400 nm excitation.

| $Ba^{2+}$ doping concentration (moL) | CIE$x$ | CIE$y$ |
|---|---|---|
| 0.00 | 0.3149 | 0.6348 |
| 0.02 | 0.3099 | 0.6418 |
| 0.04 | 0.2934 | 0.6545 |
| 0.05 | 0.2865 | 0.6600 |
| 0.06 | 0.2739 | 0.6623 |
| 0.07 | 0.2703 | 0.6647 |
| 0.08 | 0.2659 | 0.6666 |
| 0.09 | 0.2650 | 0.6677 |

**Table S3.** Chromaticity coordinates (*x*, *y*) of SBLAO:$Eu^{2+}$ with varying $Ba^{2+}$ doping concentrations (*x*) in the CIE 1931 color space under 450 nm excitation.

| **$Ba^{2+}$ doping concentration (moL)** | **CIE*x*** | **CIE*y*** |
|---|---|---|
| 0.00 | 0.3530 | 0.6093 |
| 0.02 | 0.3486 | 0.6158 |
| 0.04 | 0.3243 | 0.6361 |
| 0.05 | 0.3130 | 0.6456 |
| 0.06 | 0.3008 | 0.6491 |
| 0.07 | 0.2965 | 0.6527 |
| 0.08 | 0.2905 | 0.6564 |
| 0.09 | 0.2902 | 0.6570 |

**Table S4.** PL quantum yield and absorption efficiency as a function of $Ba^{2+}$ concentration (*x*) under 405 nm excitation.

| **$Ba^{2+}$ doping concentration (moL)** | **Internal quantum yield** | **Absorption efficiency** | **External quantum yield** |
|---|---|---|---|
| 0.00 | 0.3196 | 0.5260 | 0.1681 |
| 0.04 | 0.3303 | 0.5601 | 0.1850 |
| 0.05 | 0.3482 | 0.5657 | 0.1970 |
| 0.06 | 0.3562 | 0.5754 | 0.2049 |
| 0.07 | 0.3611 | 0.6010 | 0.2171 |
| 0.08 | 0.3116 | 0.5742 | 0.1789 |
| 0.09 | 0.3106 | 0.5361 | 0.1665 |

**Table S5.** PL quantum yield and absorption efficiency as a function of $Ba^{2+}$ concentration ($x$) under 450 nm excitation.

| **$Ba^{2+}$ doping concentration (moL)** | **Internal quantum yield** | **Absorption efficiency** | **External quantum yield** |
|---|---|---|---|
| 0.00 | 0.2691 | 0.4469 | 0.1203 |
| 0.04 | 0.3035 | 0.4853 | 0.1473 |
| 0.05 | 0.3051 | 0.5248 | 0.1601 |
| 0.06 | 0.3159 | 0.5159 | 0.1630 |
| 0.07 | 0.3332 | 0.5273 | 0.1757 |
| 0.08 | 0.3090 | 0.5195 | 0.1605 |
| 0.09 | 0.3003 | 0.4354 | 0.1307 |

**Table S6.** Chromaticity coordinates ($x$, $y$) of SBLAO:$Eu^{2+}$ with varying $Eu^{2+}$ doping concentrations ($y$) in the CIE 1931 color space under 400 nm excitation.

| **$Eu^{2+}$ doping concentration (moL)** | **CIE*x*** | **CIE*y*** |
|---|---|---|
| 0.002 | 0.2755 | 0.6479 |
| 0.005 | 0.2691 | 0.6581 |
| 0.010 | 0.2667 | 0.6664 |
| 0.015 | 0.2643 | 0.6692 |
| 0.020 | 0.2643 | 0.6699 |
| 0.030 | 0.2644 | 0.6684 |

**Table S7.** The detailed fitting results of PL lifetime [τ(μs)] for SBLAO:$Eu^{2+}$.

| Monitored wavelength (nm) | $A_1$ | $\tau_1$ | $A_2$ | $\tau_2$ | $\tau_{avg}$ | $R^2$ |
|---|---|---|---|---|---|---|
| 490 | 228.4580 | 0.1216 | 330.7674 | 0.4961 | 0.4419 | 0.995 |
| 500 | 257.1753 | 0.0909 | 390.6773 | 0.4906 | 0.4472 | 0.995 |
| 510 | 235.5049 | 0.1026 | 426.5144 | 0.5280 | 0.4868 | 0.996 |
| 520 | 215.5618 | 0.1411 | 419.3310 | 0.5817 | 0.5328 | 0.996 |
| 530 | 196.8571 | 0.1692 | 450.3407 | 0.6213 | 0.5733 | 0.996 |
| 540 | 232.3833 | 0.1601 | 540.8211 | 0.6397 | 0.5932 | 0.996 |
| 550 | 261.8886 | 0.1109 | 611.0644 | 0.6408 | 0.6042 | 0.997 |
| 565 | 191.1444 | 0.1979 | 535.8546 | 0.7276 | 0.6808 | 0.996 |
| 580 | 232.2769 | 0.1832 | 615.2828 | 0.8127 | 0.7634 | 0.997 |
| 600 | 180.9121 | 0.2413 | 617.7595 | 0.9340 | 0.8853 | 0.997 |

**Table S8.** Chromaticity coordinates (*x*, *y*) of SBLAO:$Eu^{2+}$ with varying $Eu^{2+}$ doping concentrations (*y*) in the CIE 1931 color space under 450 nm excitation.

| $Eu^{2+}$ doping concentration (moL) | CIE*x* | CIE*y* |
|---|---|---|
| 0.002 | 0.3132 | 0.6278 |
| 0.005 | 0.2995 | 0.6433 |
| 0.010 | 0.2930 | 0.6539 |
| 0.015 | 0.2889 | 0.6583 |
| 0.020 | 0.2874 | 0.6602 |
| 0.030 | 0.2880 | 0.6583 |